Plasmonics (2020) 15:1439–1449
https://doi.org/10.1007/s11468-020-01169-9

The Optical Properties of Individual Silver Nanoparticles in Ag/Ag_2O Composites Synthesized by Oxygen Plasma Treatment of Silver Thin Films

Kamal Kayed [1]

Received: 22 January 2020 / Accepted: 31 March 2020 / Published online: 17 April 2020
© Springer Science+Business Media, LLC, part of Springer Nature 2020

Abstract
In this work, we present a more complete description of the optical properties of the silver nanoparticles formed in silver oxide thin films. Ag/Ag_2O composites were synthesized by treating silver thin films manufactured by thermal evaporation method with oxygen plasma afterglow. The results showed that exposing silver thin films to oxygen plasma afterglow leads to a monocrystalline structure of silver oxide. Consequently, the relationship between the crystal size and the characteristics of the plasmon optical absorption peaks was studied. A slight degradation of plasmon peaks of the individual silver nanoparticles was observed. We suggested that this degradation might be due to the mutual interaction between the individual silver nanoparticles located near the Ag_2O grain shell and the larger silver nanoparticles in neighboring grains. We found that the degree of degradation is related to the Ag_2O grain size. On the other hand, the origin of each fluorescence peak in the Raman spectra of the prepared films was determined.

Keywords Silver oxide · Thin film · Plasmons · Thermal evaporation · Oxygen plasma afterglow · Raman spectroscopy

Introduction

The increased interest in the synthesis and characterization of plasmonic silver nanoparticles (AgNPs) loaded semiconductor films (AgNPs/semiconductor composites) is due to the unique modifications to the optical properties of the semiconductor material caused by the silver nanoparticles that are mainly related to the surface plasmon resonance (SPR) of silver nanoparticles. In this direction, the use of silver is promising because of its tunable and strong SPR from the visible to near infrared spectral regions [1–3]. The resonance effect occurs due to light-driven collective oscillations of conduction electrons in metallic Ag nanoparticles [4–7], or in other words, due to the interaction of the incident light with the electron density surrounding AgNPs [8].

AgNP doping systems find various applications in many fields such as surface plasmon, optics, electronic devices, photonics, catalysis, photography, biosensing, photocatalytic technique, catalyst, surface-enhanced Raman scattering, solar cells, sensor, optical data storage medium, and plasmon circuitry [9–28]. Each of these applications requires special engineering of AgNPs plasmonic response that depends on their shape, size, dielectric environment, and on mutual electromagnetic interactions among adjacent particles [29].

In Ag/Ag_2O composites, any agglomeration in the Ag plasmonic system due to the nature of material processes used can have an effect on the measured fluorescence emission. Many previous works [30, 31] confirmed that, both, the bandwidth and the position of the plasmon absorption band are strongly depending on the Ag_2O particle size. The silver nanoparticle fluorescence emissions show different characters with changing excitation wavelength [32]. Zheng and Dickson [33] found that only the small silver clusters synthetic by photoreduction method could yield strong fluorescence; on other hand, they found that the larger nanoparticles synthetic through reduction with $NaBH_4$ were essentially non-fluorescent. Maali et al. [34] reported that, in the case of spin-coated silver nanoparticles, the coupling of silver and silver oxide clusters controls the luminescent properties of individual silver particles.

Investigating the relationship between the silver oxide nanoparticle size and the characteristics of the plasmon optical absorption peaks is very important, because this relationship is the basis for the engineering design of Ag/Ag_2O composites,

✉ Kamal Kayed
khmk2000@gmail.com

[1] Department of Physics, Faculty of Science, Damascus University, Damascus, Syria

which make them suitable for specific applications. In this work, we show that obtaining a monocrystalline structure helps to obtain a good evaluation of the relationship between the crystal size and the characteristics of the plasmon optical absorption peaks in Ag/Ag_2O composites synthesized by oxygen plasma treatment of silver thin films. In addition, we highlight an unprecedented contribution that includes the ability to obtain information on the size of silver oxide nanoparticle from the optical absorption spectra of the individual silver nanoparticle surface plasmons.

Experimental

Sample Preparation

Pure Ag thin films (99.99%) with thickness of 316 nm were deposited at room temperature onto thoroughly cleaned n-type Si (100) and glass substrates from a high-purity Ag (99.99%) target by using thermal evaporation unit (JSM200) at a low work pressure of 5×10^{-4} Pa. The substrate was placed above the source in the direction of silver vapor flux. The target current was 225 A. The duration of the deposition process was 15 min. Each deposited films was placed in an evacuated Pyrex tube and then was exposed to a reactive oxygen plasma afterglow (OPA) stream at specific plasma power in order to oxidize the silver atoms. The O_2 plasma was generated using Microwave SAIREM GMP 20 KEDS. More details about the plasma generation system are explained in previous works [35–37]. Table 1 contains plasma exposure conditions for each sample.

Sample Characterization

Crystallite structure of the films was measured by X-ray diffraction (XRD) using (Stoe StadiP) transmission X-ray diffractometer employing a Cu $K\alpha_1$ (λ = 1.54060 Å) source. The vibrational modes present in the films were determined using Micro Raman Jobin-Yvon (LabRAM HR) with 514.5 nm laser excitation source. Scanning electron microscopy (TSCAN, Vega\\XMU) with SEM HV of 20 kV was performed to determine surface morphology and the thickness of the films. The optical transmittance and absorption spectra were recorded with a UV–Vis spectrophotometer (Cary 5000).

Results and Discussion

Figure 1 shows the SEM images of the prepared samples. It is clear from this figure that sample A (P = 250 W) has a structure composed of porous sphere-shaped clusters of nanoparticles. In the case of sample B (P = 500 W), we notice a high degree of clustering associated with an important reduction in porosity. These clusters combine to form a branch chain structure. It can be seen that the films treated at higher microwave plasma powers (samples C (P = 750 W) and D (P = 1000 W)) have columnar structures with larger clusters compared with the rest of the samples. On the other hand, as plasma power is increased to 1250 W (sample E), there is a significant reduction in the degree of clustering in addition to the disappearance of the columnar structures and an increase in porosity. In comparison with sample A, it can be observed that sample E consists of uniform clusters of smaller sizes with a lower porosity ratio. Consequently, the dramatic changes in the structure when applying plasma energy of 1250 W may be due to Ag_2O decompose to metallic Ag and O_2.

X-ray diffraction measurements were carried out on the silver oxide thin films. The XRD profiles of these samples are shown in Fig. 2. As seen in this figure, strong X-ray diffraction peak situated at $2\theta = 33.3°$ in all spectra. This peak is related to the (111) crystal plane of cubic-Ag_2O phase (CSM card no. 75-1532). This peak is dominant in the XRD spectra of the samples B, C, and D, so the oxide layers in these samples are monocrystalline. The intensity of cubic-Ag_2O phase peak (the ratio between the area and the full width at half maximum (FWHM)) increases with increasing of

Table 1 The plasma exposure conditions for each sample

Sample code	Distance from the discharge center (cm)	Plasma power (W)	Plasma pressure (Pa)	Plasma processing time (min)
A	25	250	300	30
B	25	500	300	30
C	25	750	300	30
D	25	1000	300	30
E	25	1250	300	30

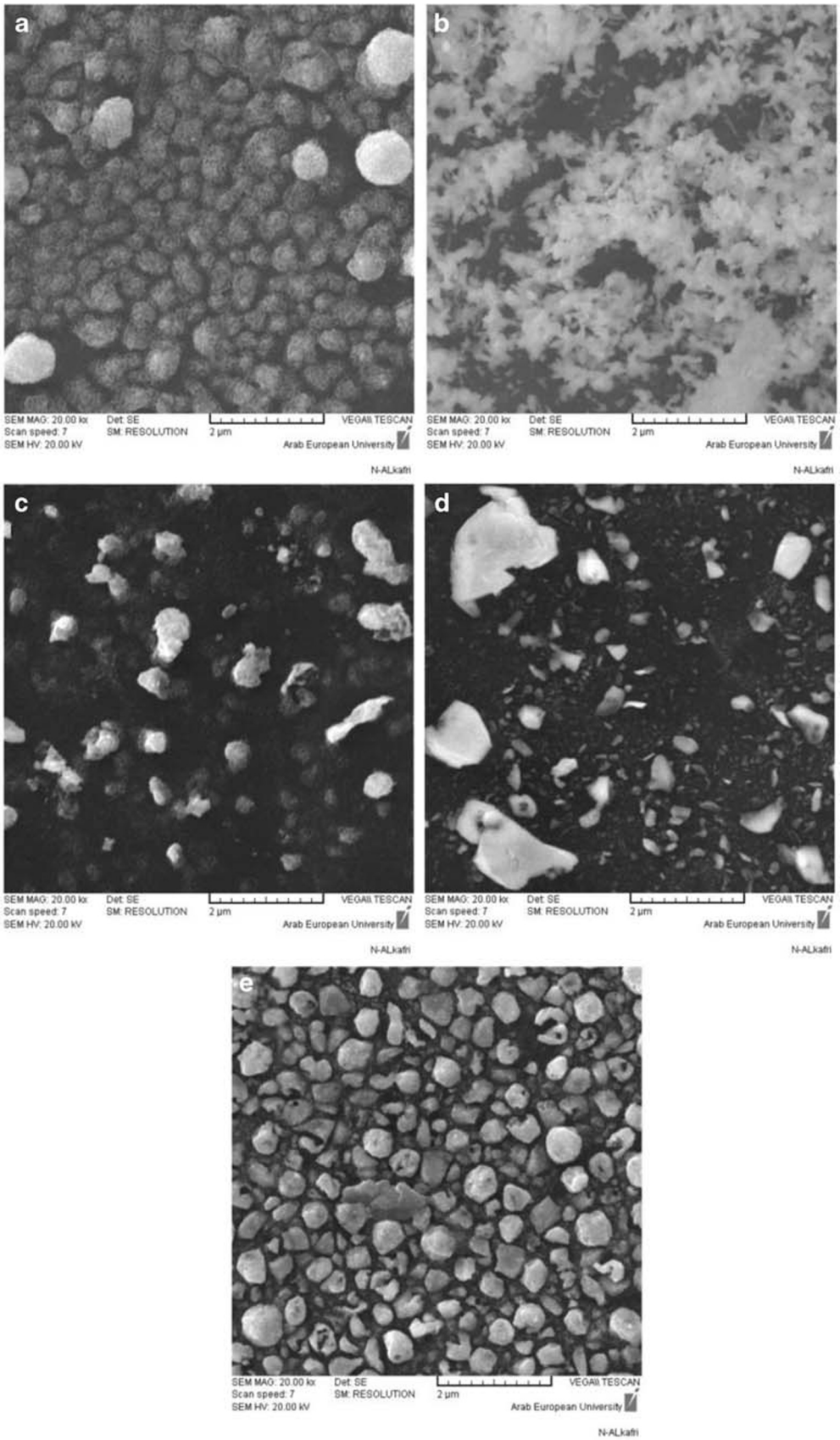

Fig. 1 The SEM images of the prepared samples

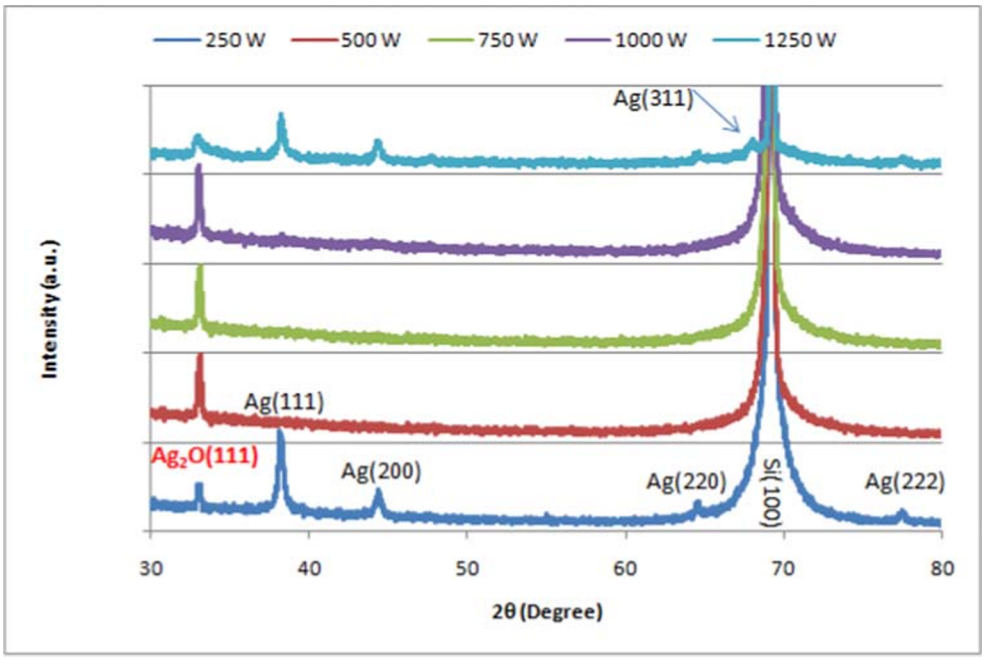

Fig. 2 The XRD spectra of the prepared samples

the plasma power in the region from 250 to 1000 W (Fig. 3). Otherwise, the treatment with plasma power of 1250 W leads to a decrease in the intensity of this peak, indicating the decomposition of Ag_2O to metallic Ag and O_2. Decomposition processes explain the appearance of the cubic silver peaks in the spectrum of the sample E (CSM card no. 87-597). These peaks also appear in the spectrum of the sample A where oxygen content is low compared with other samples. When using a plasma power of 1250 W, oxygen ions in the plasma stream obtain kinetic energy that enables them to breakdown Ag–O bonds when they collide with the newly formed silver oxide molecules.

On other hand, the grain size (D) of Ag_2O nanoparticles was estimated from XRD spectra by using the Scherrer equation [38].

$$D = \frac{K\lambda}{\beta\cos\theta} \tag{1}$$

where K is the Scherrer constant ($K = 0.89$), λ is the X-ray's wavelength, β is the full width of half maximum of

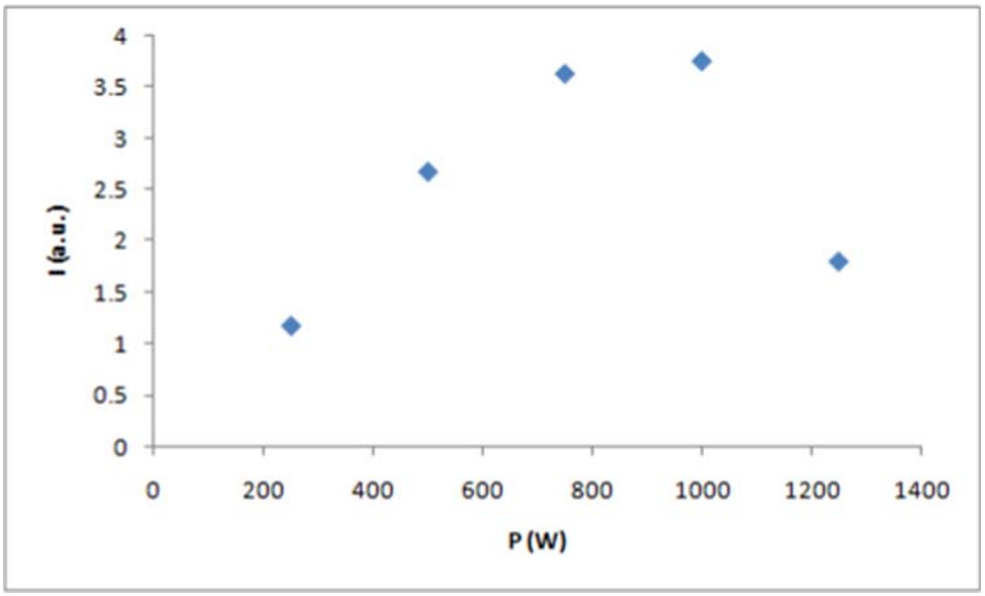

Fig. 3 The XRD peak intensity of the (111) crystal plane of cubic-Ag_2O phase as a function of plasma power

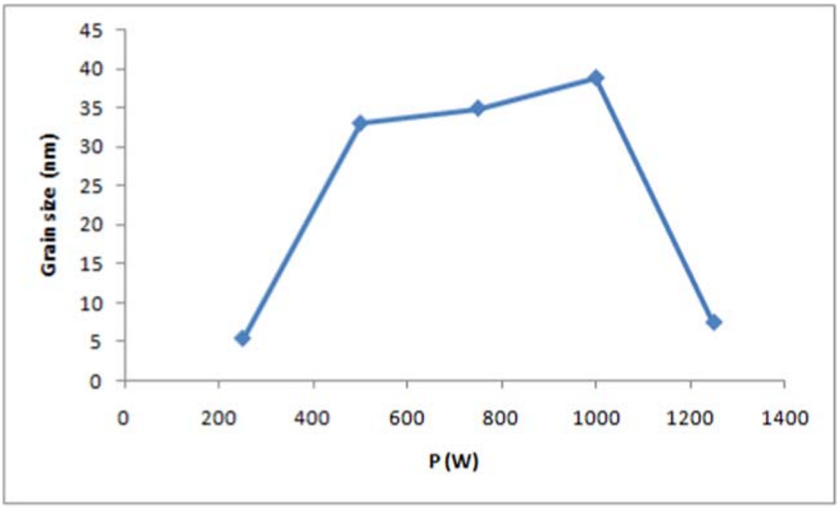

Fig. 4 The average grain size of Ag_2O particles as a function of plasma power

the Ag_2O diffraction peak, and θ is the diffraction angle. The grain size was found to be in the range 5.3–38.8 nm. Figure 4 illustrates the grain size as a function of microwave plasma power. In this figure, one observes a strong grain size dependence on the plasma power where the grain size increases with plasma power lower than 1250 W. However, a dramatic decrease in grain size occurs when applying a plasma power of 1250 W.

The optical absorption spectra of the oxygen plasma–treated Ag thin films are shown in Fig. 5. We notice that, outside the surface plasmon absorption region ($\lambda > 500$ nm), the optical absorption is almost equal for all oxygen-rich films (samples B, C, and D), with a value of about 72%. On the other hand, the films with metallic structure (samples A and E) have lower absorption, which decreases with increasing porosity. In the region ($\lambda < 500$ nm), spectra spacing of oxygen-rich samples as a result of appearance of plasmon absorption bands can be observed. The formation of these bands contributes to making absorption more sensitive to the oxygen content in the film. We noticed that for all spectra, this region contains the following contributions:

(i) A relative intense plasmon absorption peak located approximately at $\lambda = 308$ nm, which is related to the individual silver nanoparticles. By looking at Fig. 5, it can be seen that this peak has two adjacent maxima, which means that this peak is the result of overlapping two peaks (peak 1 and peak 2). In other words, there is a slight degradation of the plasmon absorption peak belonging to the individual silver nanoparticles.

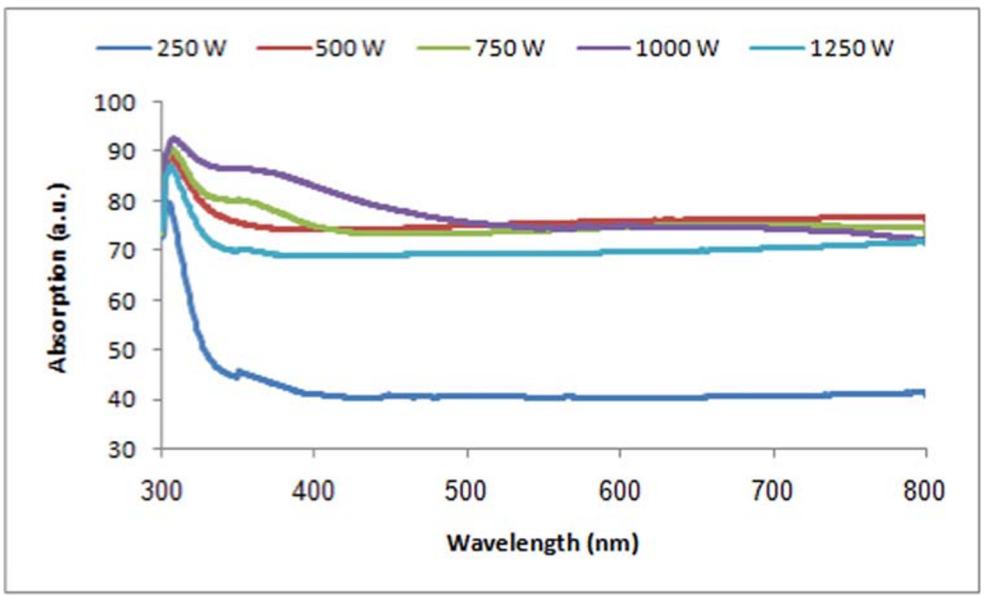

Fig. 5 The optical absorption spectra of the prepared Ag_2O thin films

(ii) A wide plasmon absorption peak (peak 3) located around λ = 343 nm is due to the surface plasmon resonance of larger Ag nanoparticles. This peak is more pronounced in the spectra of samples C and D.

In order to characterize the three peaks mentioned above, a fitting process was performed for each peak adoption of the Gaussian and Lorentzian shape. The output of the fitting process is illustrated in Fig. 6. It can be seen that the plasma power has significant effects on the main characteristics of each peak (position, FWHM, and intensity).

The calculated intensity for each peak (integrated peak area) as a function of plasma power has been shown in Fig. 7. We found that the P_3 peak intensity increased with increasing of plasma power in the region from 250 to 1000 W. This trend is associated with the decrease of intensity of both P_1 and P_2 peaks. An opposite behavior is obtained when a power of 1250 W is applied. This may be related to the decrease in both the Ag–O bond fraction and Ag_2O particle grain size at this point (Figs. 3 and 4).

Figure 8 shows the relative intensity of the P_1 and P_2 peaks (the ratio p_2/p_1) as a function of plasma power. In comparison with Fig. 4, we notice that both the grain size and the p_2/p_1 ratio have opposite behaviors with the increase of plasma power. Therefore, it is useful to investigate the relationship between the grain size and the p_2/p_1 ratio (Fig. 9).

It is obvious that, with the exception of sample (A) which has metallic nature (due to its low oxygen content), the ratio p_2/p_1 decreases as the grain size increases, and this is associated with increased oxygen content in the film. We have found that, with the exception of sample (A), our data fit well with the following equation:

$$p_2/p_1 = \alpha - \beta . x^2 \quad (2)$$

where $\alpha = (4.652)$ and $\beta = (0.0001)$.

This equation is amazing because it predicts the existence of a strong relationship between the topographical characteristics (particle size) and the optical properties of surface plasmons (the degradation ratio p_2/p_1). This equation predicts that the ratio p_2/p_1 decreases as the grain size increases, and that the P_2 peak will disappear when the grain size becomes equal to 68.21 nm. In addition, based on this equation, it can be expected that in the case of the super-smooth structure ($x =$ 0 nm), the p_2/p_1 ratio becomes equal to 4.652 nm.

The interpreting of this equation requires determining the origin of the peaks P_1 and P_2. With this respect, our perception is that the P_1 peak belongs to the individual silver atoms located inside the grain, which are free

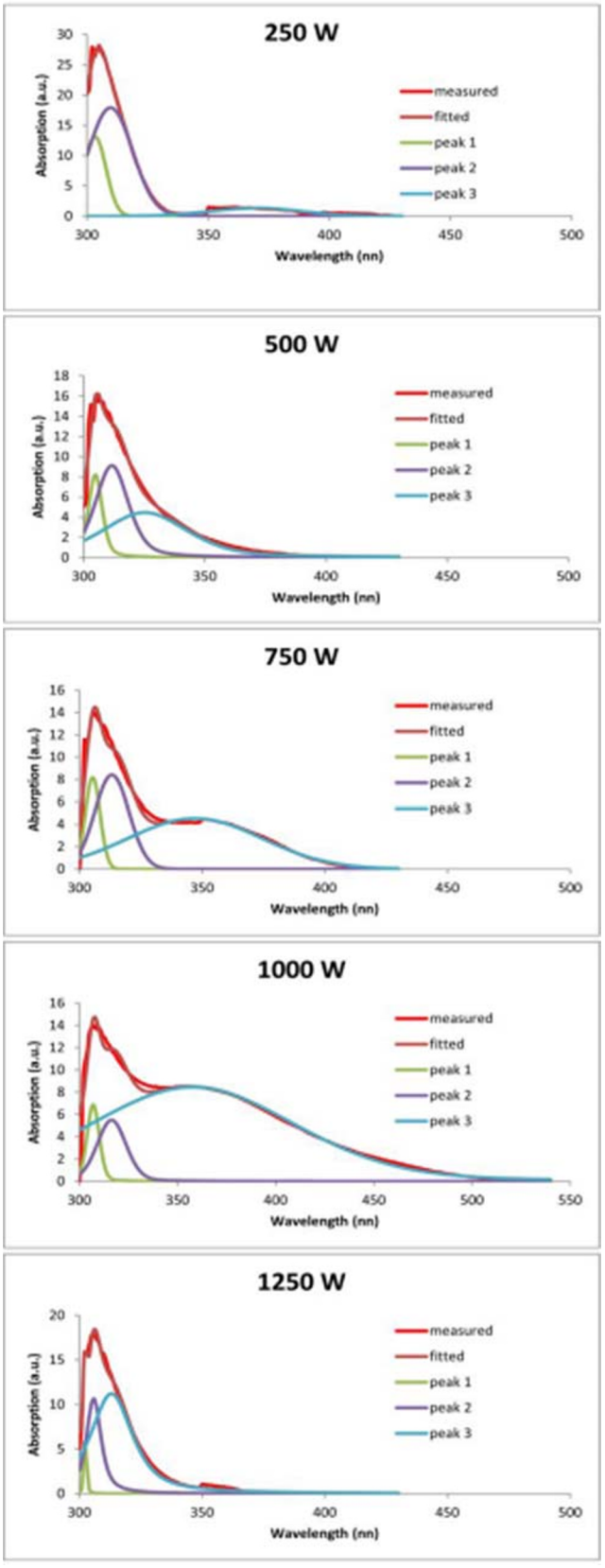

Fig. 6 The deconvoluted Plasmon absorption peaks for the prepared samples

atoms that do not interact with silver configurations in the neighboring grains. While the peak P_2 is formed as a result of the presence of individual silver atoms located on the grain boundary layer, which are slightly affected by silver configurations in the neighboring grains. Consequently, it is expected that the intensity of this peak will decrease when the area of gaps between the grain and the neighboring grains increase (the film structure becomes porous). The amount of the intensity decreases depend on the grain size. This is because as the grain size increases, the area of the gaps between the grain and the surrounding grains increases. The area of these gaps (pores) is directly proportional to the grain cross-sectional area, which in turn is proportional to x^2, where x is the grain size or the grain diameter. The increase in the pore area leads to a decrease in the number of the silver configurations surrounding the grain and consequently a reduction in the intensity of the external effects on the silver atoms of the type P_2. We conclude that, the term $-\beta.x^2$ that apparent in Eq. (2) represents the decreasing in the ratio p_2/p_1 due to the formation of grains with grain size (x).

In Fig. 10, it is observed that in the plasma power range of 250 to1000 W, increasing plasma power causes an asymmetric broadening of P_3 peak. This broadening is associated with the incorporation of oxygen in the silver network. A dramatic decrease in the FWHM of P_3 peak occurs at the power of 1250 W due to the significant reduction in the oxygen content at this power. In the case of P_1 and P_2 peaks, increased plasma power is associated with a slight decrease in the width of these peaks.

Figure 11 shows P_1, P_2, and P_3 peak positions as function of plasma power. We notice that when a power of 500 W is applied, a significant blue shift occurs in the position of P_3 peak while maintaining an almost constant value for the full width at half maximum of this peak (Fig. 10). This shift occurs because the film acquires the characteristics of semiconductor due to incorporation of additional amounts of oxygen into the silver film and the forming of Ag–O bounds. It is clear that the positions of P_1 and P_2 peaks (which belong to individual silver atoms) are not affected by this transformation. In another hand, red shifts occur when increasing the plasma power in the range 250–1000 W for the peaks P_1 and P_2 and in the range 500–1000 W for the peak P_3. This shifts associate with increasing the full width at half maximum of the P_3 peak, while the widths of the peaks P_1 and P_2 remain almost constant (Fig. 10). Previous works [39, 40] show that this type of shift occurs because the increase of %Ag content leads to the decrease of the average distance between the nanoparticles, which red shifts the SPR peak due to the interparticle coupling effect on SPR. In our case, the factor that increases is the concentration of the large Ag nanoparticles (peak 3 in Fig. 7). In addition we can also distinguish that blue shift occurs in the position associated with a decrease in width for each peak when applying a plasma power of 1250 W. This shift is distinguished from other shifts, as it is associated with decreasing grain size (Fig. 4). This type of shift occurs due to decreasing of the large Ag nanoparticle concentration and to quantum size effects [41].

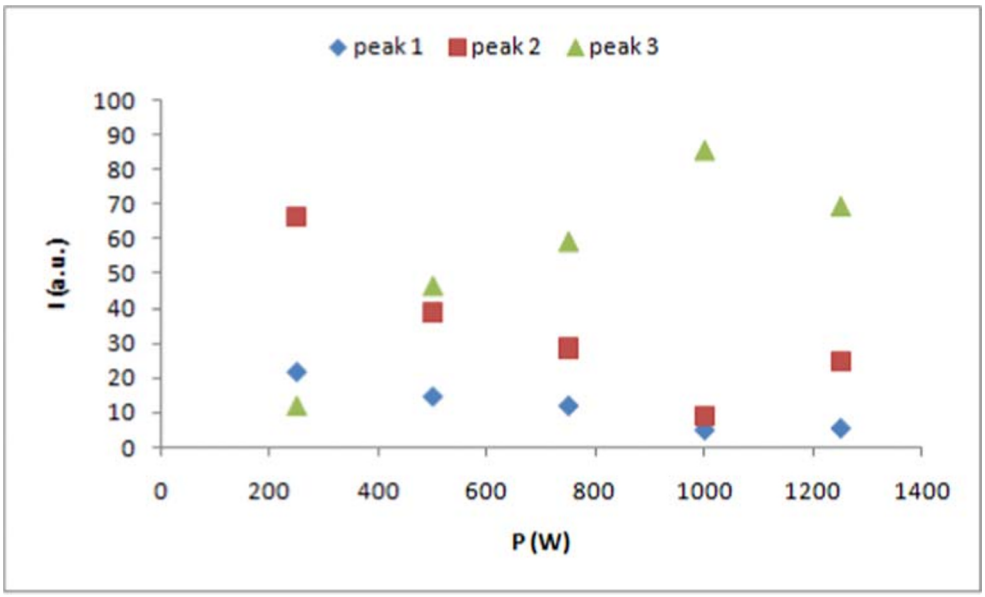

Fig. 7 The relative area of the plasmon response peaks as functions of plasma power

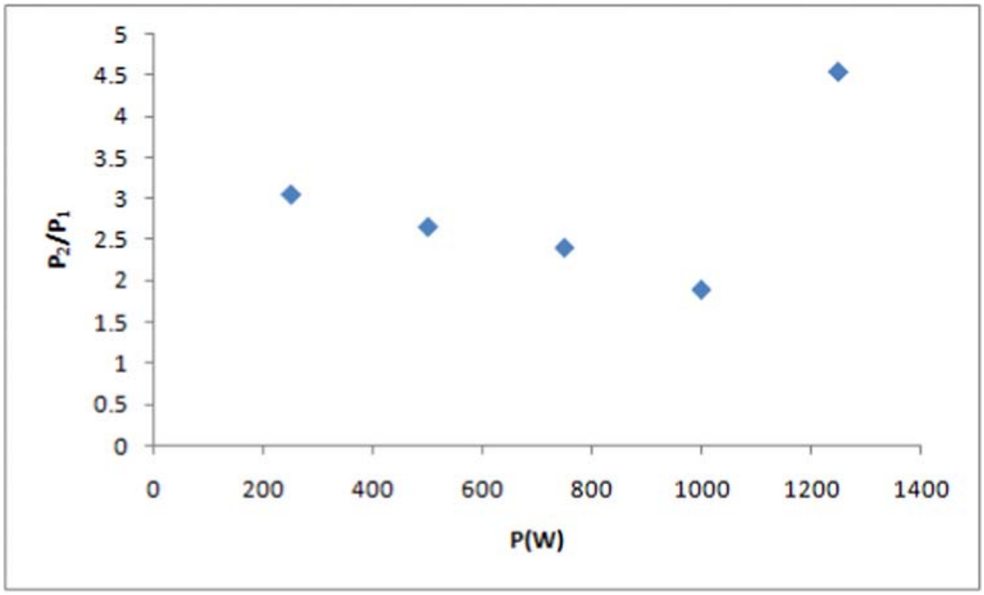

Fig. 8 The p_2/p_1 ratio as a function of plasma power

Figure 12 shows the variation of Raman spectra with plasma power. We notice that there are no characteristic peaks in the spectrum of the sample treated at 250 W. In the spectra of other samples, the broad band extending from 400 to 600 cm^{-1} is may be attributed to the presence of Ag–O bonds with different vibration modes [42, 43]. The presence of metallic silver may be the reason for not obtaining clear and separate peaks in this range. In another hand, by comparing with Fig. 3, we notice that, in Fig. 12, the maximum intensity of each Raman spectrum is proportional to the film oxygen content.

Our aim here is not to prove the formation of Al–O bonds because this was accomplished based on X-ray diffraction spectra (Fig. 2), but rather to investigate the emergence of fluorescence peaks formed due to the interaction of the laser beam with silver nanoparticles. In this regard, we observed the emergence of two major fluorescence peaks (α and β peaks) which are indicated in Fig. 12 (The arrows indicate the boundaries of the β band for each spectrum.). The α peak is located on 992.83 cm^{-1} with a FWHM of about 18 cm^{-1}. We notice that, when moving from the bottom to the top of

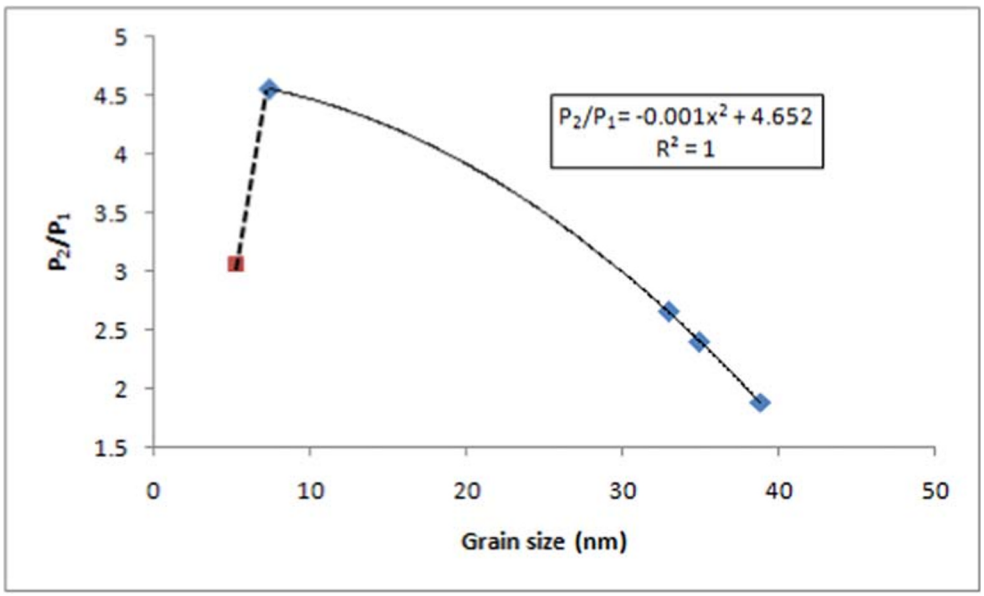

Fig. 9 The p_2/p_1 ratio as a function of grain size

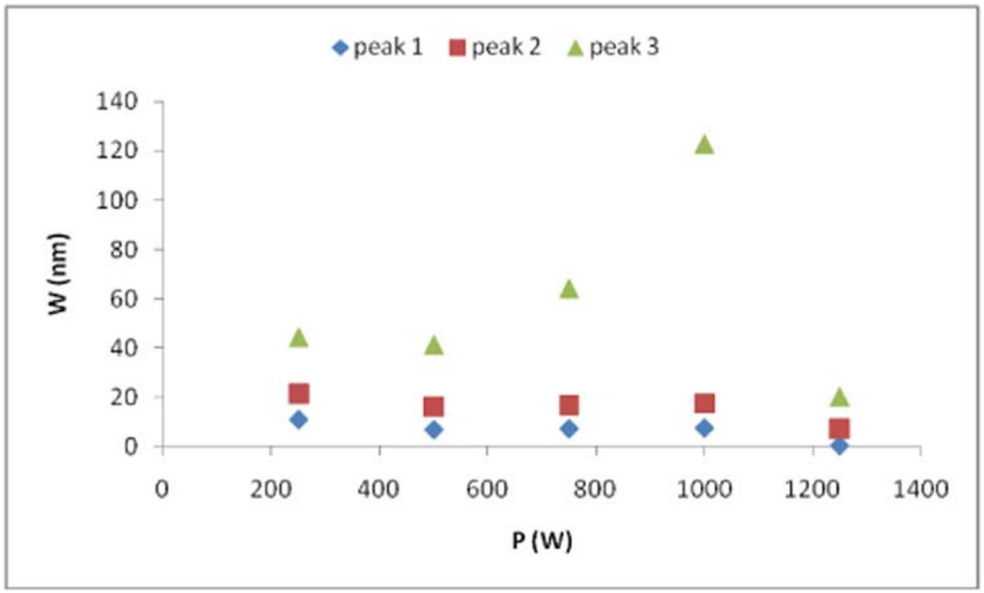

Fig. 10 The full widths at half maximum of the three surface plasmon resonance peaks as functions of plasma power

Fig. 12, the β band swells and expands which causes it to overlap with the peak α. By comparison between Figs. 6 and 12, we noticed that the growth of the individual silver nanoparticle peak (the sum of P_1 and P_2 peaks) is associated with the growth of the α peak in Raman spectrum, as well as the growth of the P_3 peak associated with the growth of β peak in Raman spectrum. Therefore, we conclude that α peak concerns the vibrations of individual silver atoms, while β peak belongs to the larger silver nanoparticles.

The α peak in the spectrum of the B sample has a small spectral width (18 cm^{-1}) and appears clearly without overlapping with any other peak. This peak disappears in the spectra of the silver-rich samples (samples A, D). In samples with high oxygen content, α peak overlaps with β peak, and this makes it unclear. The unique spectral characteristics of our samples (especially sample B) make the method of preparing these samples promising in the field of the optical storage mediums, which are also called plasmon memories and are expected to have more capacity than the conventional optical storage medium [26].

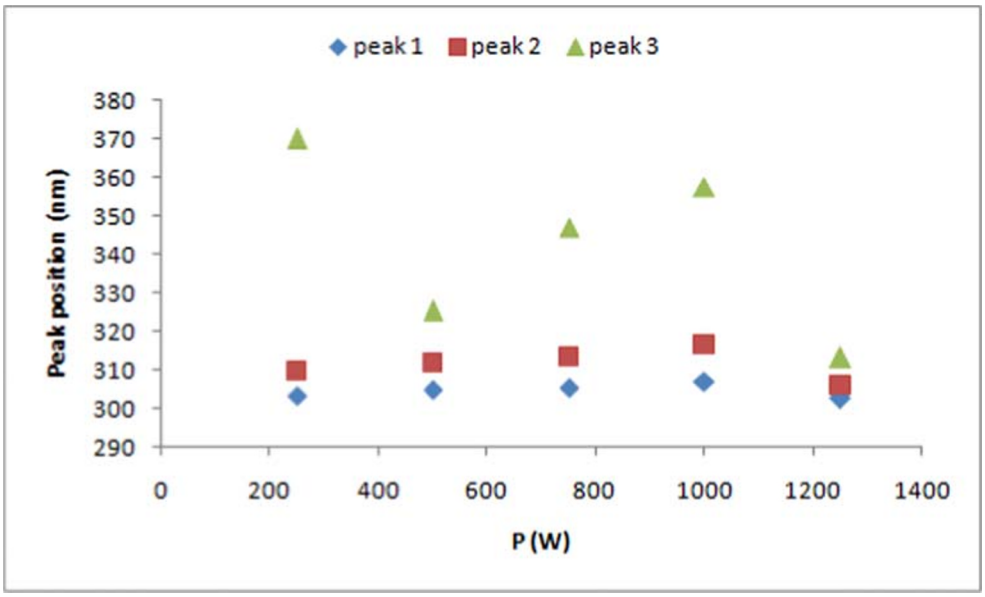

Fig. 11 The positions of the three surface plasmon resonance peaks as functions of plasma power

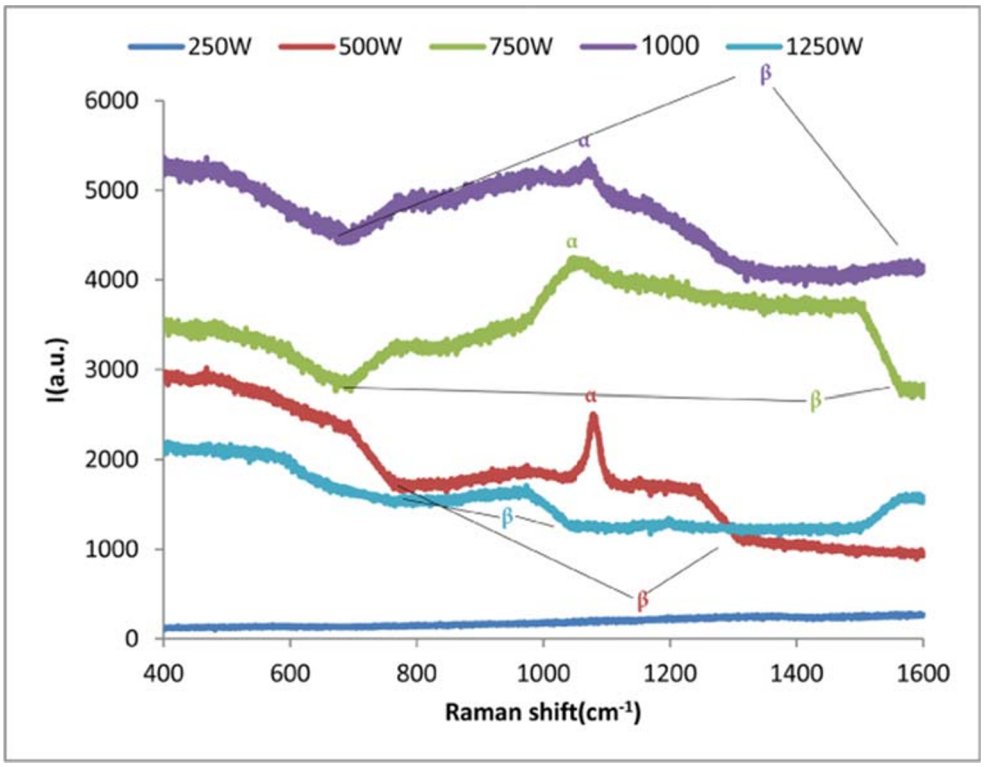

Fig. 12 Raman scattering spectra of the prepared thin films

Conclusions

In this work, we used the oxygen plasma treatment of silver thin films for the preparation of high quality silver oxide (Ag_2O) thin films having controlled structure on the nanoscale. The optical and structural properties of the prepared films were investigated where we obtained unique results, which we summarize in the following points:

1. Exposing silver thin films to oxygen plasma afterglow leads to a monocrystalline structure of silver oxide (cubic-Ag_2O phase).
2. The oxygen plasma power has significant effects on the main characteristics of each plasmon resonance peak (position, FWHM, and intensity).
3. A slight degradation of plasmon peaks of the individual silver nanoparticles was observed. We suggested that this degradation might be due to the mutual interaction between the individual silver nanoparticles located near the Ag_2O grain shell and the larger silver nanoparticles in neighboring grains. We found that the degree of degradation is related to the Ag_2O grain size.
4. We found that, the majority of samples displayed a strong emission peak in Raman spectrum centered on 992.83 cm^{-1} with a FWHM of about 18 cm^{-1} related to individual silver nanoparticles.
5. The fluorescence peaks of the individual silver nanoparticles indicate that our samples appear to have potential as materials capable of supporting optical storage medium mechanisms.

Acknowledgments The author would like to thank the University of Damascus and the Syrian Atomic Energy Commission for providing the facility to carry out this research. He would also like to thank Dr. A. Alkhawwam for the assistance during working on the Microwave SAIREM GMP 20 KEDS system.

References

1. Sun W, Hong R, Liu Q, Li Z, Shi J, Tao C, Zhang D (2019) SERS-active Ag–Al alloy nanoparticles with tunable surface plasmon resonance induced by laser ablation. Opt Mater Opt Mater 96:109298
2. Ding SY, Yi J, Li JF, Ren B, Wu DY, Panneerselvam R, Tian ZQ (2016) Nanostructure-based plasmon-enhanced Raman spectroscopy for surface analysis of materials. Nat Rev Mater 16036:1–16
3. Chan YF, Zhang CX, Wu ZL, Zhao DM, Wang W, Xu HJ, Sun XM (2013) Ag dendritic nanostructures as ultrastable substrates for surface-enhanced Raman scattering. Appl Phys Lett 102:183118
4. Madhavi V, Kondaiah P, Mohan Rao G (2018) Influence of silver nanoparticles on titanium oxide and nitrogen doped titanium oxide thin films for sun light photocatalysis. Appl Surf Sci 436:708–719
5. Low J, Yu J, Jaroniec M, Wageh S, Al-Ghamdi AA (2017) Heterojunction photocatalysts. Adv Mater 29:1601694
6. Li J, Fang W, Yu C, Zhou W, Zhu L, Xie Y (2015) Ag-based semiconductorphotocatalysts in environmental purification. Appl Surf Sci 358:46–56
7. Gomathi Devi L, Kavitha R (2016) A review on plasmonic metal–TiO2composite forgeneration, trapping, storing and dynamic vectorial transfer ofphotogenerated electrons across the Schottky junction in a photocatalyticsystem. Appl Surf Sci 360:601–622

8. Maruno S (2019) Surface plasmon spectroscopy of thin composite films of Au nanoparticles and PEDOT:PSS conjugated polymer. Org Electron 64:154–157
9. Detsri E, Popanyasak J (2015) Fabrication of silver nanoparticles/polyaniline composite thin films using layer-by-layer self-assembly technique for ammonia sensing. Colloids Surf A: Physicochem Eng Aspects 467:57–65
10. Dubas ST, Pimpan V (2008) Green synthesis of silver nanoparticles for ammonia sensing. Talanta 76:29–33
11. Fujiwara Y, Kobayashi Y, Kita K, Kakehashi R, Noro M, Katayama JI, Otsuka K (2008) Ag nanoparticle catalyst for electroless Cu deposition and promotion of its adsorption onto epoxy substrate. J Electrochem Soc 155:377–382
12. Li Y, Yao L, Song QW, Newton E (2006) Antimicrobial effect of surgical masks coated with nanoparticles. J Hosp Infect 62:58–63
13. Biswanath M, Moumita M (2009) Nonvolatile memory device based on Ag nanoparticle: characteristics improvement. Appl Phys Lett 94:233–236
14. Chiyah B, Kayed K (2018) Effect of annealing temperature on the structural and optical properties of silver oxide thin films prepared by thermal evaporation with subsequent annealing. IJNeaM 11: 305–310
15. Yang GW, Li H (2008) Sonochemical synthesis of highly monodispersed and size controllable Ag nanoparticles in ethanol solution. Mater Lett 62:2189–2191
16. Li S, Gao B, Wang Y, Jin B, Yue Q, Wang Z (2019) Antibacterial thin film nanocomposite reverse osmosis membrane by doping silver phosphate loaded graphene oxide quantum dots in polyamide layer. Desalination. 464:94–104
17. Zhao WB, Zhu JJ, Chen HY (2003) Photochemical synthesis of Au and Ag nanowires on a porous aluminum oxide template. J Cryst Growth 258:176–180
18. Dubas ST, Pimpan V (2008) Humic acid assisted synthesis of silver nanoparticles and its application to herbicide detection. Mater Lett 62:2661–2663
19. S.T. Dubas, Preparation of silver nanoparticle thin films for sensing application (Ph.D. thesis), Department of Material Science, Chulalongkorn University,Bangkok, Thailand, 2007
20. Harinee S, Muthukumar K, Dahms HU, Koperuncholan M, Vignesh S, Banu RJ, Ashok M, James RA (2019) Biocompatible nanoparticles with enhanced photocatalytic and anti-microfouling potential. Int Biodeterior Biodegradation 145:104790
21. Huang LM, Wen TC (2007) One-step synthesis of silver nanoparticles and poly(2,5-dimethoxyaniline) in poly(styrene sulfonic acid). Mater Sci Eng A445–446:7–13
22. Filippo E, Serra A, Manno D (2009) Poly(vinyl alcohol) capped silver nanoparticles as localized surface plasmon resonance-based hydrogen peroxide sensor. SensActuators B: Chem 138:625–630
23. Ling L, Feng Y, Li H, Chen Y, Wen J, Zhu J, Bian Z (2019) Microwave induced surface enhanced pollutant adsorption and photocatalytic degradation on Ag/TiO2. Appl Surf Sci 483:772–778
24. Mahapatra SS, Karak N (2008) Silver nanoparticle in hyperbranched polyamine: synthesis, characterization and antibacterial activity. Mater Chem Phys 112:1114–1119
25. Wang Y (2006) A convenient route to polyvinyl pyrrolidone/silver nanocomposite by electrospinning. Nanotechnology 17:3304–3307
26. Wadayama H, Okabe T, Taniguchi J (2018) Fabrication of multilayered structure of silver nanorod arrays for plasmon memory. Microelectron Eng 193:47–53
27. Li M, Wang Y, Xing Y, Zhong J (2020) P123-assisted preparation of Ag/Ag2O with significantly enhanced photocatalytic performance. Solid State Sci 99:106062
28. Uğur Ş, Akaoğlu C, Kucukkahveci E (2019) A study on film formation and fluorescence enhancement of PS latex/AgNPs composites depending on AgNPs content and annealing. Colloids Surf A Physicochem Eng Asp 573:40–56
29. Ren J, Tilley RD (2007) Preparation, self-assembly, and mechanistic study of highly monodispersed nanocubes. J Am Chem Soc 129: 3287–3291
30. Chiua Y (2003) Fabrication and nonlinear optical properties of nanoparticle silver oxide films. J Appl Phys 94:1996–2001
31. Lamprecht B (2000) Ultrafast plasmon dynamics in metal nanoparticles, Institute for Experimental Physics, Karl-Franzens University of Graz, Australia, Ph.D thesis
32. Jian Z, Xiang Z, Yongchang W (2005) Electrochemical synthesis and fluorescence spectrum properties of silver nanospheres. Microelectron Eng 77:58–62
33. Zheng J, Dickson RM (2002) Individual water-soluble dendrimer-encapsulated silver nanodot fluorescence. J Am Chem Soc 124: 13982
34. Maalia A, Cardinal T, Treguer-Delapierre M (2003) Intrinsic fluorescence from individual silver nanoparticles. Phys E 17:559–560
35. Alkhawwam A, Abdallaha B, Kayed K, Alshoufi K (2011) Effect of nitrogen plasma afterglow on amorphous carbon nitride thin films deposited by laser ablation. Acta Phys Pol A 120:545–551
36. Kayed K (2010) Synthesis and properties of carbon nitride and boron nitride thin films prepared by different techniques, Damascus University Syria, Damascus, PhD thesis
37. Kayed K (2018) Effect of nitrogen plasma afterglow on the (1000–1800) cm−1 band in FTIR spectra of amorphous carbon nitride thin films. Spectrochim Acta A Mol Biomol Spectrosc 190:253–258
38. Scherrer P (1912) Bestimmung der inneren Struktur und der Größe vonKolloidteilchen mittels Röntgenstrahlen, in: Kolloidchemie Ein Lehrbuch,Springer, pp. 387–409
39. Su KH, Wei QH, Zhang X, Mock JJ, Smith DR, Schultz S (2003) Interparticle coupling effects on plasmon resonances of nanogold particles. Nano Lett 3:108–1090
40. Choi BH, Lee HH, Jin S, Chun S, Kim SH (2007) Characterization of the optical properties of silver nanoparticle films. Nanotechnol. 18:075706
41. Mandal SK, Roy RK, Pal AK (2002) Surface plasmon resonance in nanocrystalline silver particles embedded in SiO_2 matrix. J Phys D Appl Phys 35:2198–2205
42. Geoffrey I, Waterhouse N, Graham A, Bowmaker, Metson JB (2001) The thermal decomposition of silver (I, III) oxide: a combined XRD, FT-IR and Raman spectroscopic study. Phys Chem Chem Phys:3838–3845
43. Raju NRC, Kumar KJ, Subrahmanyam A (2009) Physical properties of silver oxide thin films by pulsed laser deposition: effect of oxygen pressure during growth. J Phys D Appl Phys 42:135411 (6pp)

Publisher's Note Springer Nature remains neutral with regard to jurisdictional claims in published maps and institutional affiliations.